Particuology 15 (2014) 77–81

Contents lists available at ScienceDirect

Particuology

journal homepage: www.elsevier.com/locate/partic

Short communication

Carbonate-salt-based composite materials for medium- and high-temperature thermal energy storage

Zhiwei Ge[a,c], Feng Ye[a], Hui Cao[b], Guanghui Leng[a], Yue Qin[d], Yulong Ding[a,b,e,*]

[a] State Key Laboratory of Multiphase Complex Systems, Institute of Process Engineering, Chinese Academy of Sciences, Beijing 100190, China
[b] Institute of Particle Science & Engineering, University of Leeds, Leeds LS2 9JT, UK
[c] University of Chinese Academy of Sciences, Beijing 100049, China
[d] School of Engineering and Technology, China University of Geosciences, Beijing 100083, China
[e] Centre for Cryogenic Energy Storage, University of Birmingham, Edgbaston, Birmingham, B15 2TT, UK

ARTICLE INFO

Article history:
Received 12 June 2013
Received in revised form 22 August 2013
Accepted 3 September 2013

Keywords:
Thermal energy storage
Composite materials
Microstructure
Thermal conductivity
Phase change material

ABSTRACT

This paper discusses composite materials based on inorganic salts for medium- and high-temperature thermal energy storage application. The composites consist of a phase change material (PCM), a ceramic material, and a high thermal conductivity material. The ceramic material forms a microstructural skeleton for encapsulation of the PCM and structural stability of the composites; the high thermal conductivity material enhances the overall thermal conductivity of the composites. Using a eutectic salt of lithium and sodium carbonates as the PCM, magnesium oxide as the ceramic skeleton, and either graphite flakes or carbon nanotubes as the thermal conductivity enhancer, we produced composites with good physical and chemical stability and high thermal conductivity. We found that the wettability of the molten salt on the ceramic and carbon materials significantly affects the microstructure of the composites.

1. Introduction

Thermal energy storage plays a vital role in the effective and efficient use of renewable energy resources and industrial waste heat. Keys to thermal storage technology include materials' development and heat exchange during charge and discharge processes. Molten salts are among the most promising phase change materials (PCMs) for thermal energy storage at medium- and high-temperatures. However, applications of molten salts as PCMs are often hampered by chemical incompatibility (such as corrosion of containers) and low thermal conductivities (Guillot et al., 2012; Zhao & Wu, 2011). To overcome these limitations, composites containing carbon allotropes as thermal conductivity enhancing materials (TCEMs) have been proposed. Mixing carbon allotropes with molten salts followed by compression (Acem, Lopez, & Palomo Del Barrio, 2010; Lopez, Acem, & Palomo Del Barrio, 2010) or infiltration of molten salts into a prefabricated carbon (such as graphite foam) (Tammer, 2008) have been shown to be effective approaches for significantly increasing the thermal conductivity of the composites. However, poor dispersion of the carbon in liquid molten salts often leads to the separation of the carbon from the bulk liquid phase of molten salts. Although infiltration of liquid molten salts into prefabricated blocks of carbon materials can avoid this separation issue, the resulting composites are often unable to retain sufficient PCMs within their structures at medium- and high-temperatures, leading to leakage of molten salts during solid–liquid phase change, and hence a decrease in thermal energy storage density of the composites (Pincemin, Olives, Py, & Christ, 2008). Relatively poor wetting between carbon materials and liquid molten salts is an important reason for the leakage and phase separation; the difference in densities of the salts and carbons is also a contributing factor.

In this paper, we introduce microstructured composite materials (intended for medium- and high-temperature applications), consisting of a molten salt-based PCM, a ceramic skeleton as PCM carrier, and a carbon-based thermal conductivity enhancer. We show that the PCM is encapsulated within the composite microstructure, and, the thermal conductivity can be substantially enhanced.

2. Experimental

2.1. Raw materials and composite fabrication

The PCM used in this work was a eutectic carbonate molten salt ($LiNaCO_3$) made from sodium carbonate (Na_2CO_3, Beijing Chemical Works) and lithium carbonate (Li_2CO_3, Sinopharm

* Corresponding author at: State Key Laboratory of Multiphase Complex Systems, Institute of Process Engineering, Chinese Academy of Sciences, Beijing 100190, China.
E-mail addresses: ylding@mail.ipe.ac.cn, y.ding@leeds.ac.uk (Y. Ding).

1674-2001/$ – see front matter © 2013 Published by Elsevier B.V. on behalf of Chinese Society of Particuology and Institute of Process Engineering, Chinese Academy of Sciences.
http://dx.doi.org/10.1016/j.partic.2013.09.002

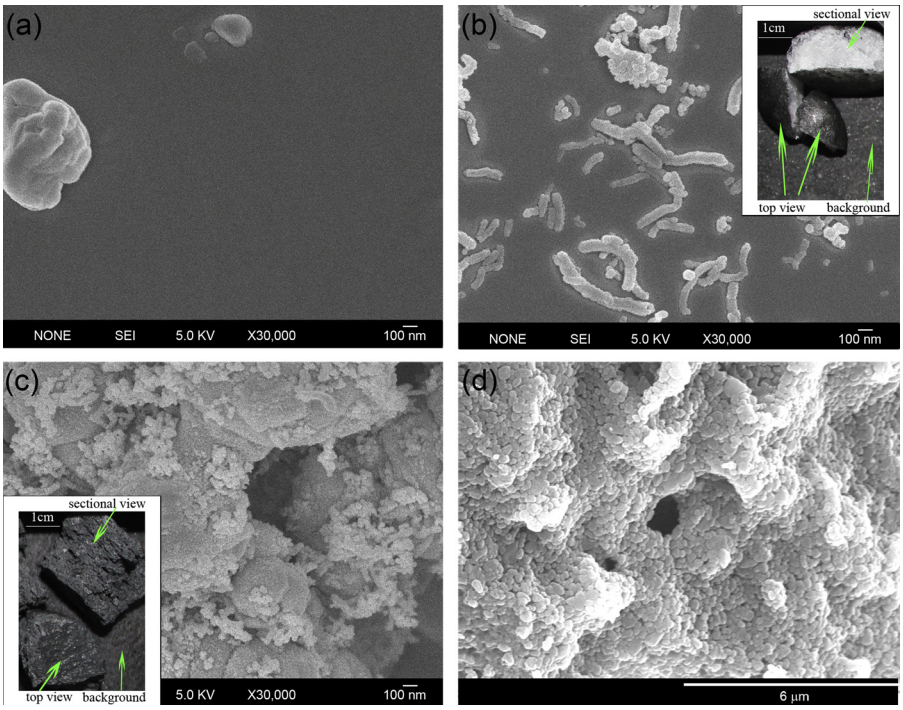

Fig. 1. Micrographs of (a) PCM ($LiNaCO_3$), (b) 1PCM/0.01CNTs; inset is a macroscopic optical image. (c) 1PCM/1MgO/0.015CNTs; inset is a macroscopic optical image, and (d) 1PCM/1MgO. Note that in the optical images, the PCM appears white and the CNTs are black.

Chemical Reagent Co. Ltd). Ceramic (MgO, Sinopharm Chemical Reagent Co. Ltd) and carbon materials (natural graphite flakes and carbon nanotubes (CNTs), Beijing Dk Nano Technology Co. Ltd) were chosen as the skeleton material and thermal conductivity enhancer, respectively. The eutectic salt was made by mixing thoroughly 43% Li_2CO_3 and 57% Na_2CO_3 (mass percentage) and heating the mixture to a temperature above the melting temperature. Fabrication of eutectic based composites involved three steps. First, the eutectic salt was thoroughly mixed with appropriate amounts of ceramic and carbon materials. The mixture was then shaped into disk-like green pellets by uniaxial compression. Finally, the green pellets were sintered in an electric furnace using the following heating procedure: heating from 25 to 400 °C at 5 °C/min, then from 400 to 550 °C at 1 °C/min, and holding at 550 °C for 90 min. The cooling procedure was the reverse of the heating process.

2.2. Sample characterization

The morphological and microstructural characterization of the composites was carried out by scanning electron microscopy (SEM, JSM-7100F, JEOL, Japan), and X-ray microtomography (XMT, Micro-CT200, Xradia, USA). A Laser flash apparatus (LFA 427, Netzsch, Germany) and a thermal analyzer (TG-DSC, STA 449F3 Jupiter®, Netzsch, Germany) were used to evaluate the thermophysical properties of the samples.

3. Results and discussion

3.1. Characterization of the composites

Fig. 1 shows SEM images and macroscopic digital photos of some typical samples. The PCM ($LiNaCO_3$) particles exhibit a round shape and a relatively smooth surface (Fig. 1(a)). When CNTs are added, the nanoparticles can only be found at the surface of the PCM particles, as shown in the digital photo in the upper right corner of Fig. 1(b), and almost no CNTs (dark in color) are seen within the bulk of the phase change material (white in color). The cross-sectional and top views of Fig. 1(b) show that the sample is almost semicircular, with CNTs distributed only on the surface of the PCM particles. Fig. 1(c) shows an SEM image of a composite material containing the PCM, MgO, and CNTs in a mass ratio of 1:1:0.015. MgO crystals, with diameters of 0.15–0.6 μm, are distributed uniformly on the surface of the sample. Comparing the insets in Figs. 1(b) and 1(c), we notice that that the CNTs are much better dispersed in the salt in the presence of MgO. Such structural differences between the samples with and without the MgO skeleton material are not only because of the liquid-phase-sintered microstructure (Fig. 1(d)), but are also likely to be associated with interfacial energies between the different components of the composite materials.

Fig. 2 shows XMT images of the samples of different compositons. As shown in Fig. 2(a), the PCM particle after melting and recrystallization has a round shape. Although uniaxial compression was applied during the preparation stage, many pores remain in the PCM structure; these can be attributed to the volume change of the PCM during the melting/recrystallization process. Fig. 2(b) shows the PCM containing CNTs. In this composite, the pores are larger than those in the pure PCM (Fig. 2(a)), and all the CNTs are

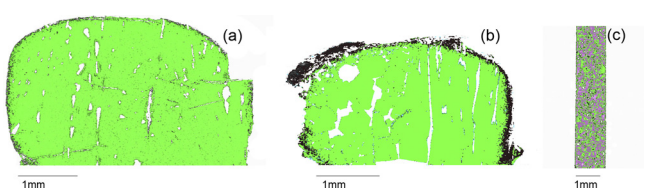

Fig. 2. XMT images of (a) PCM ($LiNaCO_3$) at slice 465, (b) 1PCM/0.01CNTs at slice 500, and (c) composite material 1PCM/1MgO/0.015CNTs at slice 531 in the XY planes. Images are obtained from segmentation of the scanned samples by thresholding with Mimics10.0 software; green, black, and pink colors represent PCM, CNTs, and MgO, respectively. (For actual colours mentioned in the text, readers are referred to the on-line web version of this article.)

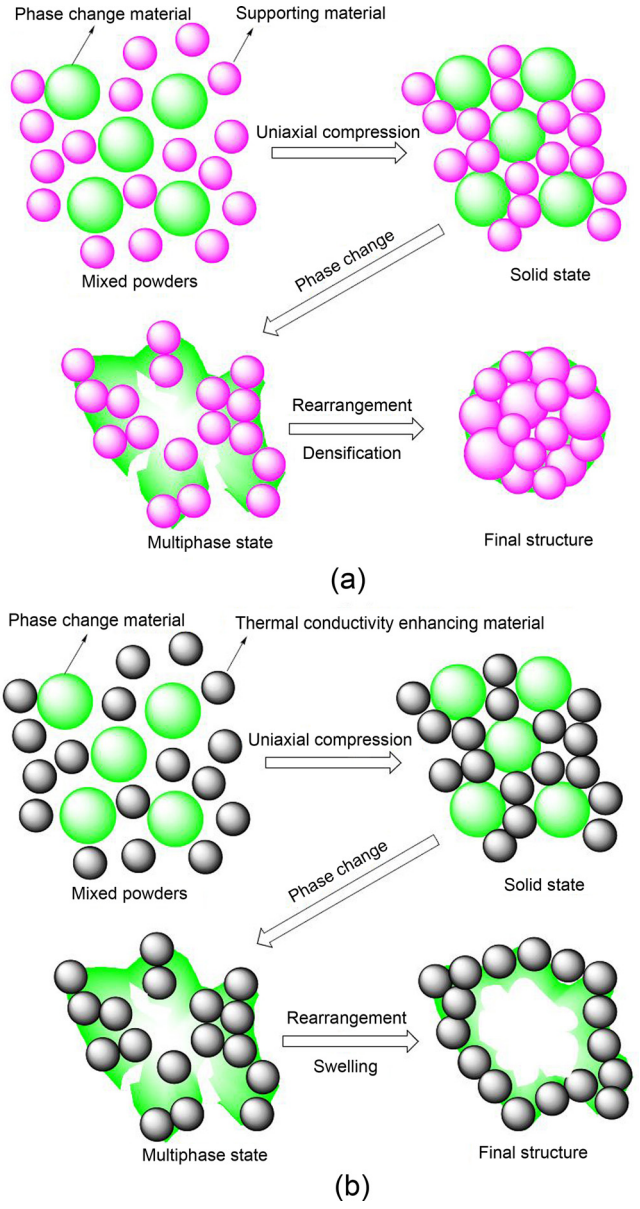

Fig. 3. Schematics of microstructure formation mechanism for (a) PCM and ceramic skeleton material, (b) PCM and thermal conductivity enhancer; green, black, and pink colors represent PCM, thermal conductivity enhancer, and ceramic, respectively.

distributed on the exterior surface of the PCM particle. Fig. 2(c) shows a composite material comprising PCM, MgO, and CNTs with a 1:1:0.015 mass ratio. The PCM and CNTs are uniformly distributed within the structure formed by the skeleton material (MgO). The XMT results are consistent with the SEM analyses shown above.

3.2. Microstructure formation

Fig. 3(a) shows a proposed microstructure formation mechanism for a composite consisting of the PCM and ceramic material. During powder mixing, pores take the form of interparticle voids. Upon uniaxial compression, the amount of void space is reduced, while the green density increases. Upon sintering, the solid phase PCM begins to turn into liquid as the temperature approaches the melting point, leading to multiphase composites with co-existing

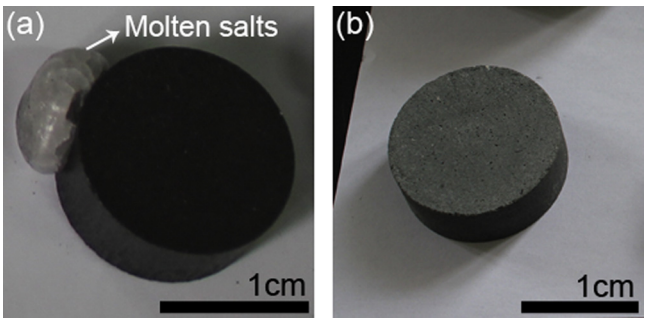

Fig. 4. Photos of composites without (a) and with (b) the ceramic material, showing that the ceramic reduces loss of molten salt from the composite.

solid, liquid, and gas phases. According to the following Young's equation:

$$\gamma_{sv} = \gamma_{sl} + \gamma_{lv} \times \cos\theta, \quad (1)$$

the wettability of the liquid phase on the solid phase is related to the contact angle (θ), which is a function of the interfacial energies (γ, where the subscripts s, l, and v correspond to the solid, liquid, and gas phases, respectively) (German, Suri, & Park, 2009; German, 2010). As ceramic materials often have a relatively high interfacial energy, a small contact angle is expected. As a consequence, the liquid PCM phase is likely to be able to wet the skeleton material, and spread on its surface to displace the solid–gas interface, and instead of forming liquid–solid and liquid–gas interfaces. At the same time, the wetting liquid provides a capillary force to pull the ceramic particles together and rearrange them to form a dense composite. This will increase the local rigidity of the structure. After sintering, the final structure consists of grains of skeleton material, bound by solidified liquid salt. Such a microstructure could prevent PCM leakage during solid–liquid phase change.

Carbon materials such as CNTs and graphite are less likely to be wetted by the liquid molten salts, even though they have sufficient surface tension to allow wetting by water ($\gamma \sim 72$ mN/m) and most organic solvents ($\gamma < 72$ mN/m) (Dujardin, Ebbesen, Hiura, & Tanigaki, 1994; Pincemin et al., 2008). This poor wettability could lead to swelling, as illustrated in Fig. 3(b), and thus forming a relatively loose, porous structure. This explains the separation of the CNTs from the bulk PCM particles when the composites contained only PCM and carbon, as discussed earlier and shown in Figs. 1(b) and 2(b).

This is also consistent with the observation that little PCM was found in composites consisting only of carbon material and PCM, as shown in Fig. 4(a). However, for the composites containing the PCM, the ceramic skeleton, and the carbon material, the rearrangement and densification of the skeleton material with the liquid molten salt can significantly restrict the swelling caused by the carbon material, allowing the formation of a uniform composite, as shown in Figs. 1(c) and 2(c), and effective encapsulation of the PCM in the composite, as shown in Fig. 4(b).

To further elucidate the influence of carbon material on the microstructure of the composite, the effects of graphite and CNT loadings within the composites were studied. Fig. 5 shows the bulk density of the samples as a function of loading of the carbon material. The bulk densities of both the graphite composites (Fig. 5(a)) and the CNT composites (Fig. 5(b)) show a turning point. The density of the sintered composites is higher than the green pellets and this tendency decreases with increasing loading of carbon, until a critical loading is reached (at the turning point). Further increase in the carbon loading leads to a significant decrease in the density of the sintered composites and a lower density than the green composites. Such behavior suggests the existence of a competing

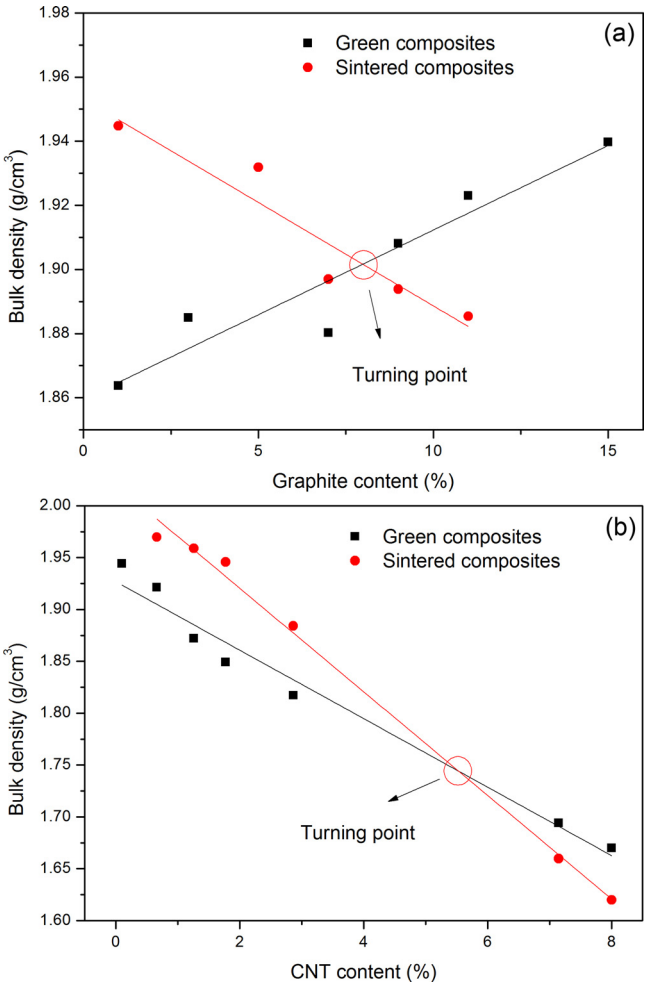

Fig. 5. Bulk density as a function of carbon content: (a) graphite and (b) CNTs.

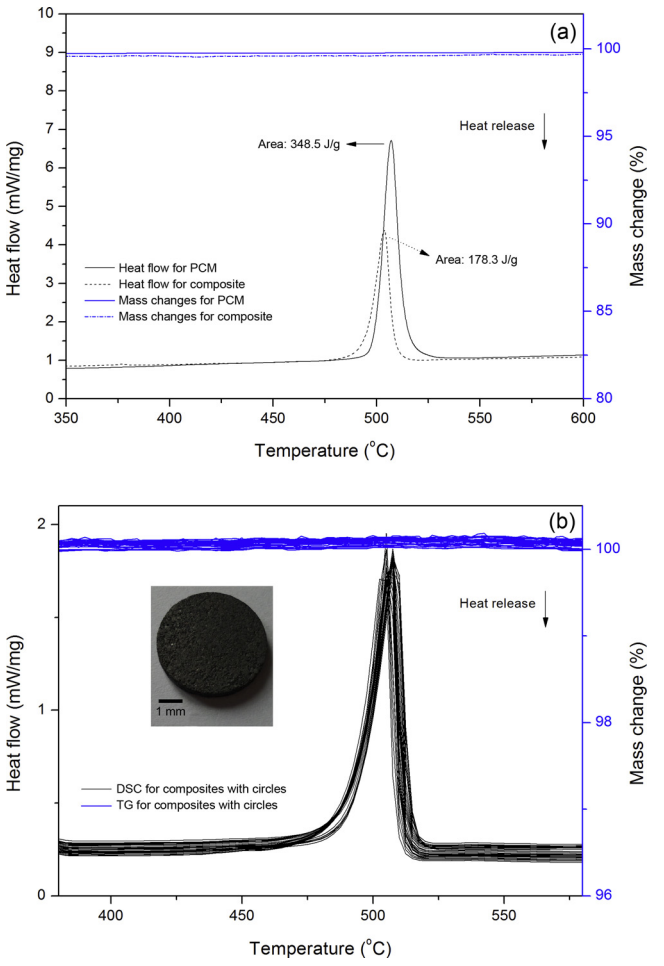

Fig. 6. TG-DSC curves for (a) the PCM and the composite, and (b) the composite over 28 thermal cycles.

process due to different wettabilities of the ceramic material and the carbon material with the liquid PCM phase. High wettability of the ceramic densifies the final composite, while poor wettability of the carbon material swells it. Inspection of Fig. 5(a and b) shows that the density at the turning point for the graphite composites is much higher than that for the CNT composites. This is probably because the layered (two-dimensional) structure of the graphite flakes makes it easier to orient the graphite perpendicularly to the compression direction (Acem et al., 2010; Yuan et al., 2012), leading to a higher composite density for graphite than that of composites containing CNTs, which have a one-dimensional hollow tubular structure.

3.3. Thermophysical properties of the composites

The TG–DSC curves for the eutectic carbonate ($LiNaCO_3$) and the composite containing graphite, $LiNaCO_3$, and MgO are given in Fig. 6. The TG curves of Fig. 6(a) show that both the PCM and the composite have good thermal stability. The DSC curves in Fig. 6(a) yield enthalpy of melting values of about 348.5 J/g for the eutectic carbonate and about 178.3 J/g for the composite. This difference is simply because there is less molten salt in the composite than in the pure molten salt, for any given sample mass. To evaluate the chemical and physical stability of the composites, thermal cycling experiments were conducted and the corresponding TG–DSC curves are plotted in Fig. 6(b); the TG curves show negligible mass change over the 28 thermal cycles, indicating that the composite material has a good thermal stability. The image in the inset of Fig. 6(b) shows that the composite has maintained its original shape after 28 thermal cycles. The chemical stability of the composite can be evaluated from the DSC curves in Fig. 6(b). No significant changes to the melting point or the heat of fusion are seen over the 28 thermal cycles.

The thermal energy that can be stored in a composite PCM material includes the latent heat of the PCM and the sensible heat of both the solid and liquid phases in the composite; the majority of the stored energy is through the latent heat. On the other hand, the thermal conductivity of the composite depends on the concentration, size, shape, orientation and spatial distribution of the thermal conductivity enhancer; the higher the concentration of the enhancer, the higher the thermal conductivity. However, a higher concentration of thermal conductivity enhancer means a lower energy storage density. As a consequence, the right balance must be struck between thermal conductivity and energy storage density requirements for a specific application. Fig. 7 plots the thermal conductivity and thermal energy storage density of the composites as a function of graphite loading. One can see that addition of carbon material can greatly enhance the thermal conductivity, with the enhancement increasing with increasing carbon loading in the composite. Thermal conductivity over 5 W/(m K) can be achieved with a carbon loading of 20%. A 10% carbon loading gives a composite with a thermal conductivity over 4.3 W/(m K) and an energy storage density over 530 kJ/kg.

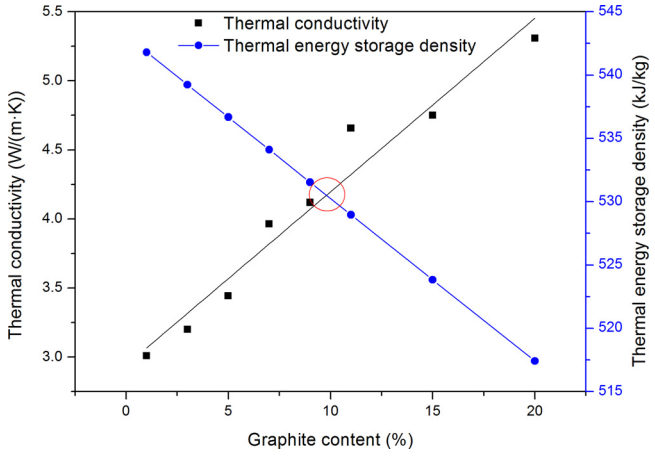

Fig. 7. Thermal conductivity and thermal energy storage density of composites as a function of graphite loading.

4. Conclusions

We investigated inorganic-salt-based composite materials for medium- and high-temperature thermal energy storage. Using a eutectic salt of lithium and sodium carbonates as the PCM, magnesium oxide as the ceramic skeleton, and carbon allotropes as the thermal conductivity enhancer, we produced composites with good physical and chemical stability and high thermal conductivity. We found that good wettability of the salt on the ceramic material densifies the composite structure, whereas poor wettability of the salt on the carbon materials swells the composite structure. The balance between such competing processes plays a key role in the properties and behaviour of the composite materials. Our results show that a 10% carbon loading gives a composite with a thermal conductivity over 4.3 W/(m K) and an energy storage density over 530 kJ/kg.

Acknowledgements

Parts of this work were supported by the Focused Deployment Project of the Chinese Academy of Sciences (KGZD-EW-302-1), Key Technologies R&D Program of China (No. 2012BAA03B03) and Natural Science Foundation of China (Grant No. 21106151), and the UK Engineering and Physical Sciences Research Council (EPSRC) under grant EP/K002252/1.

References

Acem, Z., Lopez, J., & Palomo Del Barrio, E. (2010). $KNO_3/NaNO_3$ – Graphite materials for thermal energy storage at high temperature: Part I – Elaboration methods and thermal properties. *Applied Thermal Engineering*, *30*, 1580–1585.

Dujardin, E., Ebbesen, T. W., Hiura, H., & Tanigaki, K. (1994). Capillarity and wetting of carbon nanotubes. *Science*, *265*, 1850–1852.

German, R. M., Suri, P., & Park, S. J. (2009). Review: Liquid phase sintering. *Journal of Materials Science*, *44*, 1–39.

German, R. M. (2010). Coarsening in sintering: Grain shape distribution, grain size distribution, and grain growth kinetics in solid-pore systems. *Critical Reviews in Solid State and Materials Sciences*, *35*, 263–305.

Guillot, S., Faik, A., Rakhmatullin, A., Lambert, J., Veron, E., Echegut, P., et al. (2012). Corrosion effects between molten salts and thermal storage material for concentrated solar power plants. *Applied Energy*, *94*, 174–181.

Lopez, J., Acem, Z., & Palomo Del Barrio, E. (2010). $KNO_3/NaNO_3$ – Graphite materials for thermal energy storage at high temperature: Part II – Phase transition properties. *Applied Thermal Engineering*, *30*, 1586–1593.

Pincemin, S., Olives, R., Py, X., & Christ, M. (2008). Highly conductive composites made of phase change materials and graphite for thermal storage. *Solar Energy Materials and Solar Cells*, *92*, 603–613.

Tammer, R. (2008). Energy storage for direct steam solar power plants. DISTOR Report No. SES6-CT-2004-503526.

Yuan, G., Li, X., Dong, Z., Westwood, A., Cui, Z., Cong, Y., et al. (2012). Graphite blocks with preferred orientation and high thermal conductivity. *Carbon*, *50*, 175–182.

Zhao, C. Y., & Wu, Z. G. (2011). Heat transfer enhancement of high temperature thermal energy storage using metal foams and expanded graphite. *Solar Energy Materials and Solar Cells*, *95*, 636–643.